Available online at www.sciencedirect.com
ScienceDirect
Trans. Nonferrous Met. Soc. China 34(2024) 184−193
Transactions of Nonferrous Metals Society of China
www.tnmsc.cn

Residual stresses in linear friction welding of TC17 titanium alloy considering phase fraction

Peng HE[1,2], Yun-xin WU[1,2], Tao ZHANG[1,2], Song-yi CHEN[1,2], Chen ZHANG[1,2]

1. Light Alloy Research Institute, Central South University, Changsha 410083, China;
2. State Key Laboratory of Precision Manufacturing for Extreme Service Performance, Central South University, Changsha 410083, China

Received 13 July 2022; accepted 12 April 2023

Abstract: To obtain accurate residual stresses in linear friction welding of TC17 alloy, a numerical relationship between the elastic constants and phase fraction of TC17 alloy was established. The elastic constants with gradient distribution were obtained by combining the phase fraction and introduced into the contour method. The results show that the elastic constants of TC17 alloy are positively correlated with α phase fraction and present a significant gradient distribution in the welding area with a width of about 4 mm. The relative error in calculating the welding residual stresses can be up to 36.06% if the gradient distribution of phase fraction is ignored. The corrected residual stresses in the welding area exhibit a bimodal distribution, with a peak stress of ~442 MPa located at the edge of the heat-affected zone. The results demonstrate the necessity of considering the phase fraction with gradient distribution.

Key words: linear friction welding; TC17 titanium alloy; residual stresses; phase fraction; gradient distribution

1 Introduction

TC17 (Ti−5Al−2Sn−2Zr−4Mo−4Cr) titanium alloy is a dual-phase α+β titanium alloy rich in β-stabilizing elements. It is widely used in aero-engine bladed disks (blisks) owing to its advantages, such as high strength, good fracture toughness and excellent fatigue resistance [1−4]. In molten state, the titanium alloy is highly reactive to atmospheric gases, such as nitrogen and oxygen, resulting in severe embrittlement [5,6]. As a result, traditional fusion welding of the titanium alloy requires the protection of vacuum or inert gas. Linear friction welding (LFW) is a solid-state welding technique that joins titanium alloy by applying pressure and generating frictional heat on the welding surface. Its welding temperature is below the melting point of TC17 titanium alloy, and it does not require a vacuum environment or inert gas protection. Thus, LFW has become a key technology for manufacturing the aero-engine blisks [7−9].

However, a large temperature gradient and plastic deformation occur on the welding surface during LFW, resulting in a complex distribution of residual stresses in the weldment [10,11], which affects the service life and mechanical performance of blisks. Therefore, it is essential to quantify the residual stresses after LFW. Several advanced methods, such as crack compliance method, layer removal method, and contour method, have been developed for measuring internal residual stresses [12,13]. Among them, the contour method can effectively measure the normal residual stress distribution on the cutting surface of the weldment. Its accuracy is not affected by the size of the welding area, making it effective for measuring welding residual stresses. There have been several studies on the measurement of welding residual stresses using this method. FRANKEL et al [14]

Corresponding author: Yun-xin WU, Tel: +86-13087319063, E-mail: wuyunxin@csu.edu.cn
DOI: 10.1016/S1003-6326(23)66390-3

compared the internal residual stresses in linear friction weldments between Ti-64 and Ti-6242 and found that the peak tensile stress in Ti-6242 introduced through the welding process was greater than that in Ti-64. HOSSEINZADEH et al [15] measured the internal residual stresses in Ti-64 electron beam weldments, and the tensile residual stresses were mainly concentrated within 9 mm from the weld centre. DEWALD et al [16] calculated the residual stresses in Ti-64 linear friction weldments. They found that the peak tensile stress appeared in the weld centre. GADALLAH et al [17] studied the influence of applied pressure on the internal residual stresses in linear friction welded steel sheets. The results showed that the stress gradient close to the weld centre decreased as the applied pressure increased.

In the LFW process, the welding temperature in the welding area significantly exceeds that of α/β phase transition point (890 °C) of TC17 titanium alloy, causing changes in α/β phase fraction [8], thus affecting the elastic constants of TC17. According to the characteristics of the grains, LI et al [18] and WANG et al [19] divided the weld joint of TC17 alloy into four distinct zones: the weld zone (WZ), the thermo-mechanically affected zone (TMAZ), the heat affected zone (HAZ), and the parent material zone (PMZ). In these zones, the α phase translated to β phase in varying degrees, resulting in the non-homogeneous distribution of mechanical properties. The α phase with hexagonal close-packed (HCP) crystal structure and β phase with body-centered cubic (BCC) crystal structure in titanium alloy can display different elastic constants, leading to variations in the elastic constants of titanium alloy in the LFW process [20,21]. Several studies have reported the effect of phase fraction on the elastic modulus of titanium alloy. For example, LEE and WELSCH [22] found that the elastic modulus of Ti-64 was positively related to the α phase fraction, which could be used as a sensitive indicator of phase fraction variation. OGI et al [23] showed that the elastic constants rapidly decreased around the α/β phase transition point due to the transition from α to β phase. According to CHEN et al [24], the formation of the α phase resulted in a high elastic modulus during the preparation of Ti−37Nb−6Sn alloy.

However, the measurement of the non-homogeneous elastic constants in the welding area using experiments is difficult due to the narrowness of this area. In the previous studies on residual stresses calculated with the contour method, the mechanical properties of the material were assumed to be homogeneous by neglecting those zones where the material properties changed due to the phase fraction variation. Considering the non-homogeneity of elastic constants, the authors in this study investigated the variation of α phase fraction in the welding area of TC17 titanium alloy, and introduced it into the contour method to improve the precision of measuring the welding residual stresses.

2 Relationship between elastic constants and phase fraction

2.1 Experimental procedures

The relationship between the elastic constants and phase fractions of titanium alloys was established using TA9 (Ti−0.2Pd) and TB5 (Ti−15V−3Cr−3Sn−3Al). In addition, four samples of TC17 (Ti−5Al−2Sn−2Zr−4Mo−4Cr) titanium alloy with different phase fractions were prepared to verify the relationship. The elastic modulus and shear modulus were measured at room temperature using the elastic modulus tester (IET−1600VP). The phase fractions were analyzed by X-ray diffraction (XRD, Malvern Panalytical Empyrean Alpha 1).

2.2 Elastic constants and phase fraction

At room temperature, TA9 and TB5 are mainly composed of α and β phases, respectively [25,26]. Therefore, their α phase fractions can be assumed to be 100% and 0%, respectively. The elastic and shear moduli are given in Table 1, which indicates a large difference between the moduli of different samples.

As the α phase fraction of TC17 titanium alloy increased from 55.5% to 88.7%, its elastic modulus increased from 104.35 to 120.64 GPa. Studies have shown that the isotropic elastic modulus of titanium alloy is related to the α/β phase fraction, and the loss of α phase fraction decreases elastic modulus [27,28].

2.3 Fitting results between elastic constants and phase fraction

As shown in Fig. 1, TC17 titanium alloy is considered an isotropic composite, consisting of

Table 1 Measured values of elastic constants

Material	Phase fraction/%	Elastic modulus/GPa	Shear modulus/GPa
TA9	α=100; β=0 (assumed)	130.45	46.80
TB5	α=0; β=100 (assumed)	85.67	30.42
TC17 (1#)	α=69.6; β=30.4	112.07	42.49
TC17 (2#)	α=55.5; β=44.5	104.35	41.41
TC17 (3#)	α=77.5; β=22.5	117.20	42.77
TC17 (4#)	α=88.7; β=11.3	120.64	46.23

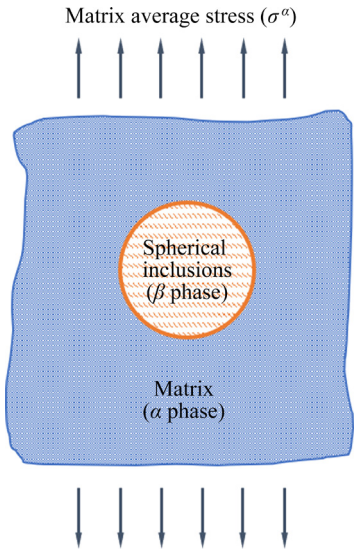

Fig. 1 Application of Mori−Tanaka model in TC17

matrix and spherical inclusions that are uniformly distributed in the matrix. Mori−Tanaka equivalent inclusion micromechanics theory [29−31] is used to calculate the elastic and shear modulus of TC17 titanium alloy with different phase fractions. Then, the following equations can be obtained:

$$K_{\mathrm{TC17}} = K_{\alpha}\left[1+\frac{(1-\eta)\left(K_{\beta}/K_{\alpha}-1\right)}{1+\eta a\left(K_{\beta}/K_{\alpha}-1\right)}\right] \tag{1}$$

$$G_{\mathrm{TC17}} = G_{\alpha}\left[1+\frac{(1-\eta)\left(G_{\beta}/G_{\alpha}-1\right)}{1+\eta b\left(G_{\beta}/G_{\alpha}-1\right)}\right] \tag{2}$$

$$E_{\mathrm{TC17}} = \frac{9K_{\mathrm{TC17}}G_{\mathrm{TC17}}}{3K_{\mathrm{TC17}}+G_{\mathrm{TC17}}} \tag{3}$$

$$a = \frac{3K_{\alpha}}{3K_{\alpha}+4G_{\alpha}} \tag{4}$$

$$b = \frac{6\left(K_{\alpha}+2G_{\alpha}\right)}{5\left(3K_{\alpha}+4G_{\alpha}\right)} \tag{5}$$

where K_{TC17}, G_{TC17}, and E_{TC17} denote the bulk, shear, and elastic moduli of TC17 titanium alloy, respectively. K_{α}, G_{α}, K_{β}, and G_{β} denote the bulk and shear moduli of α and β phases, respectively. η denotes the volume fraction of α phase.

However, preparing pure-phase TC17 titanium alloy is difficult. Therefore, K_{α}, G_{α}, K_{β}, and G_{β} can be calculated from the measured elastic and shear moduli of TA9 and TB5 at room temperature by Eq. (6):

$$\begin{cases} E_{\mathrm{TA9}} = \dfrac{9K_{\alpha}G_{\alpha}}{3K_{\alpha}+G_{\alpha}} \\ G_{\mathrm{TA9}} = G_{\alpha} \\ E_{\mathrm{TB5}} = \dfrac{9K_{\beta}G_{\beta}}{3K_{\beta}+G_{\beta}} \\ G_{\mathrm{TB5}} = G_{\beta} \end{cases} \tag{6}$$

where E_{TA9}, G_{TA9}, E_{TB5}, and G_{TB5} denote the elastic and shear moduli of TA9 and TB5 titanium alloys, respectively.

Figure 2 shows the theoretically calculated values of K_{TC17} and G_{TC17} with different α phase fractions, which indicates that they are positively correlated with α phase fraction.

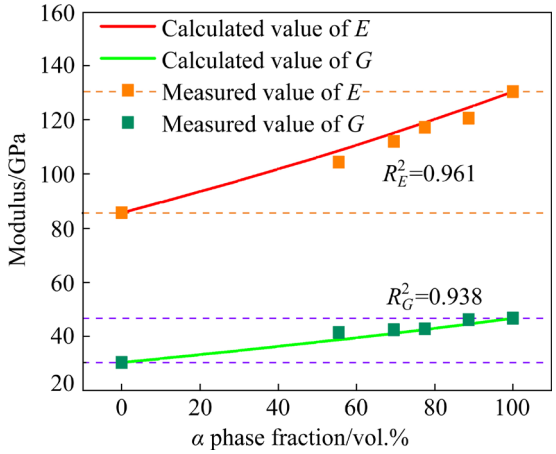

Fig. 2 Variation of TC17 elastic constants with α phase fraction

2.4 Validation of fitting results

The comparison between the calculated values of modulus (Table 2) and the experimental results (Table 1) is represented in Fig. 2, and the maximum relative errors are 4.12% and 6.25%, respectively. The result shows that the theoretical calculation can predict E_{TC17} and G_{TC17} with different α phase fractions well.

Table 2 Calculated values of elastic constants

Material	Elastic modulus/GPa	Shear modulus/GPa
TC17 (1#)	115.19	41.21
TC17 (2#)	108.65	38.82
TC17 (3#)	119.00	42.61
TC17 (4#)	124.58	44.65

3 LFW elastic constants and residual stresses

3.1 Experimental procedures

3.1.1 LFW

The workpieces made of TC17 titanium alloy (1#) as parent material (PM), with dimensions of 62 mm (length) × 75 mm (width) × 20 mm (thickness), were welded by LFW with the welding surfaces of width−thickness. Before welding, the welding surfaces were ground with a milling machine and cleaned with anhydrous ethanol. The cleaned workpieces were welded at AVIC Manufacturing Technology Institute (Beijing, China) under the welding conditions listed in Table 3. After LFW, the flash was moved. Then post-weld heat treatment (PWHT) was applied to weldments at 630 °C for 3 h, followed by air cooling.

Table 3 LFW parameters

Amplitude/mm	Frequency/Hz	Friction pressure/MPa
3	50	100

According to the position of the welding area, the metallographic specimens of 20 mm × 10 mm × 10 mm were cut perpendicular to the welding direction (Fig. 3). The specimens were ground, polished, and etched with Kroll's reagent (1% HF + 3% HNO_3 + 45% H_2O). Afterward, the specimens were analyzed using optical metallography (OM). The width of each zone can be determined through the grain topology, which guides the XRD experiment. The XRD specimens were cut from the metallographic specimens according to the width of WZ, TMAZ, HAZ, and PMZ (Fig. 3). Then, XRD specimens were ground and analyzed using the Malvern Panalytical Empyrean Alpha 1 for phase fraction. Specifically, Surfaces I, II, III, and IV, corresponding to PMZ, HAZ, TMAZ and WZ, respectively, were analyzed using XRD. To ensure the accuracy of the sampling, it is important to make sure that the cuts are made strictly according to the width of each zone.

3.1.2 Contour method

As shown in Fig. 4, the LFW weldments were cut centrally along the *xOz* plane using the DK7625P wire electric discharge machine (EDM) with 0.2 mm brass wire. The residual stresses introduced by cutting process were ignored [32]. The cutting speed was 1mm/min, and the continuity of the cutting process was maintained.

After the specimen was cut, the contour of cut surfaces was measured using the MQ8106 coordinate measuring machine (CMM) with 0.1 μm

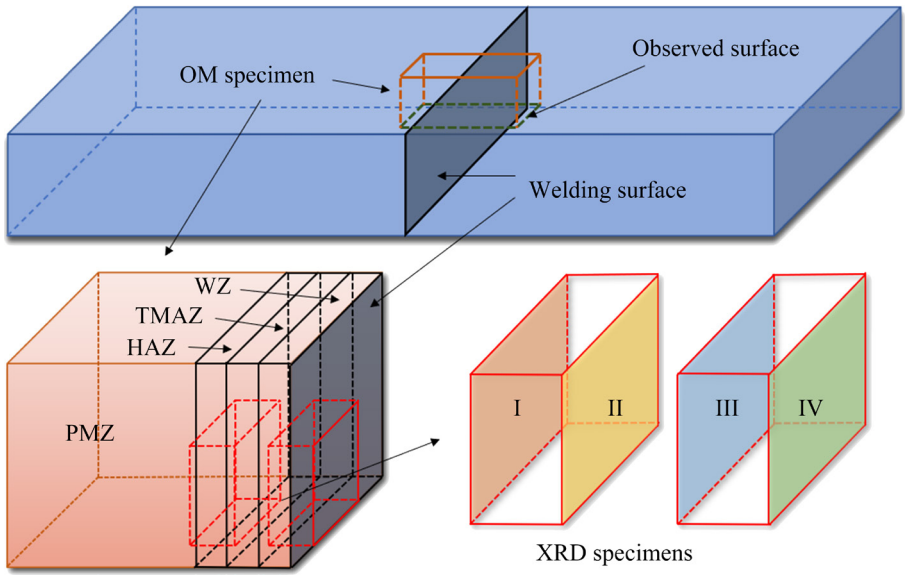

Fig. 3 Specimens obtained from LFW weldment

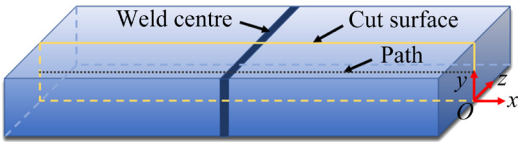

Fig. 4 Schematic diagram of cut surface

measuring resolution. Then, the raw data were processed with coordinate conversion, noise reduction and enveloping to reduce the error introduced to the system during cutting or contour measurement [33]. The measured data were applied as boundary conditions to the same-size model for finite element analysis (FEA) based on ABAQUS/standard to obtain the internal residual stresses in the weldments.

3.2 Microstructural observation

The welding area can be divided into WZ, TMAZ, HAZ, and PMZ according to the different structure characteristics, as shown in Fig. 5(a). Among them, the width of HAZ, TMAZ, and WZ are ~1000, ~500, and ~800 μm, respectively, and the rest is PMZ.

The PMZ is composed of α+β phase with a typical basket-weave structure, as shown in Fig. 5(b). The β grains are relatively coarse, with a size of 0.5−2 mm. A little massive and strip primary α_p phase can be observed in the β phase matrix, where numerous lath and needle-like secondary α_s phases are dispersed.

Under high temperature and mechanical friction condition, the grains in WZ experience dynamic reversion and recrystallization, forming equiaxed grains with a uniform grain size of 20−30 μm, as shown in Fig. 5(c). After LFW, the β phase transformed by the α phase is too late to transform back due to the large cooling rate, thus forming metastable β grains.

The grain size in TMAZ is significantly varied. As shown in Fig. 5(d), the grains are severely deformed along the metal flow direction. In TMAZ close to the WZ side, dynamic reversion and recrystallization of the β grains lead to the formation of fine equiaxed grains, which is the same in WZ. When close to the HAZ side, the α phase fraction increases significantly, and the needle-like α_s phase is diffusely distributed in β phase matrix.

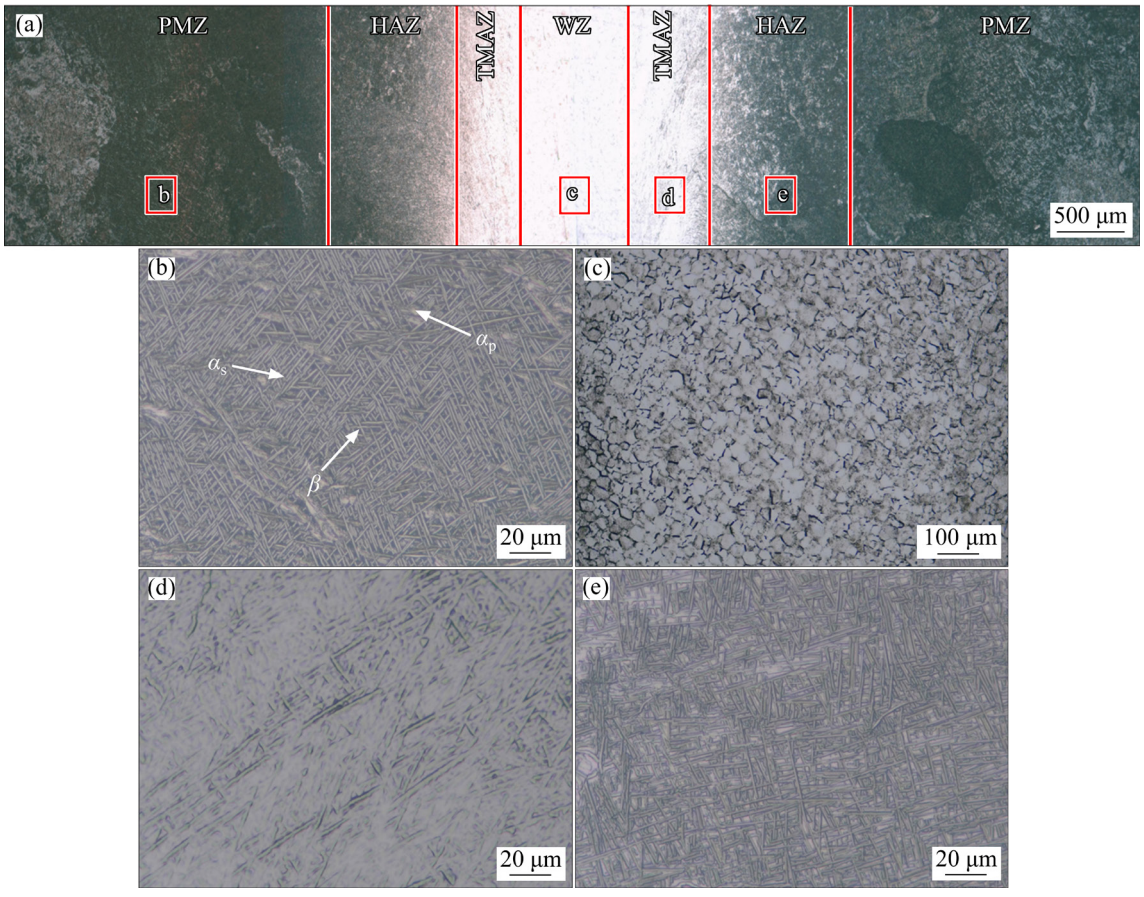

Fig. 5 Microstructure of TC17 in welding area: (a) Overall; (b) PMZ; (c) WZ; (d) TMAZ; (e) HAZ

As shown in Fig. 5(e), the grain size and morphology in HAZ are similar to those in PMZ because they are less affected by mechanics and high temperature. However, the aspect ratio of the needle-like α_s phase decreases, and a small portion of α_s phase transforms into β phase.

In conclusion, the microstructure and α/β phase fraction significantly vary in the welding area. The material properties of LFW weldments are not homogeneous.

3.3 Phase fraction with gradient distribution

Figure 6 shows the gradient distribution of α phase content in the welding area of TC17 titanium alloy. The phase transformation occurs in the welding area, with the α phase content decreasing from 69.6 vol.% in PMZ to 4 vol.% in WZ, which is consistent with the microstructural variation in the welding area. TMAZ and WZ are significantly influenced by high temperature, giving rise to a steep α phase content gradient. The α phase content increases from 63.4 vol.% to 69.6 vol.% in the range of 0.5 mm during the transition from HAZ to PMZ. The increase in α phase content might be caused by the fact that these two zones are less affected by the high temperature, and only part of the needle-like α_s transforms to β in HAZ.

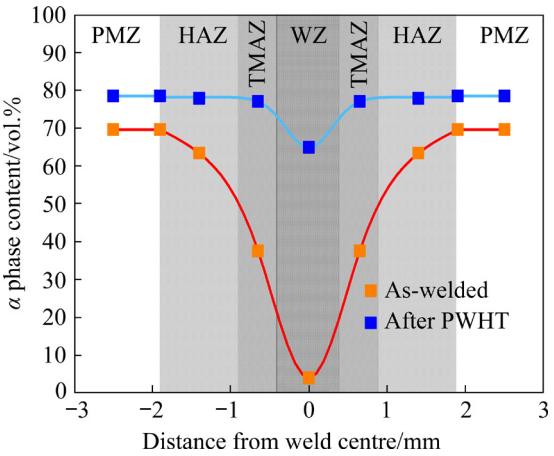

Fig. 6 Variation of phase fraction in welding area

After PWHT, the α phase content increases to different degrees in all zones and remains the lowest in WZ. The α phase content increases from 77.8 vol.% to 78.5 vol.% during the transition from HAZ to PMZ, with an insignificant difference. The α phase contents in WZ and TMAZ vary significantly, increasing from 4 vol.% to 64.9 vol.% and from 37.6 vol.% to 77 vol.%, respectively. This phenomenon is attributed to the transformation of β to α in the above zones and the precipitation of a large number of α_p and α_s with different shapes in the metastable β matrix [28,34]. The α phase content in PMZ varies from 69.6 vol.% to 78.5 vol.%, as only a tiny amount of α_s precipitates occur in β matrix [3].

3.4 Elastic constant variation

According to the analysis of the α phase fraction in the previous section, the variation in E_{TC17} and G_{TC17} in the welding area is obtained (Fig. 7), which is consistent with the trend of α phase fraction in Fig. 6. A significant difference is observed in the elastic constants in different zones. During the transition from PMZ to WZ, E_{TC17} decreases from 115.19 to 87.19 GPa, and G_{TC17} decreases from 41.21 to 30.98 GPa. After PWHT, E_{TC17} and G_{TC17} increase in all zones. Considerable variation is observed in WZ, with E_{TC17} and G_{TC17} increasing from 87.19 to 112.98 GPa and from 30.98 to 40.4 GPa, respectively. In PMZ, the overall increases in E_{TC17} and G_{TC17} are approximately 4.5 and 1.5 GPa, respectively.

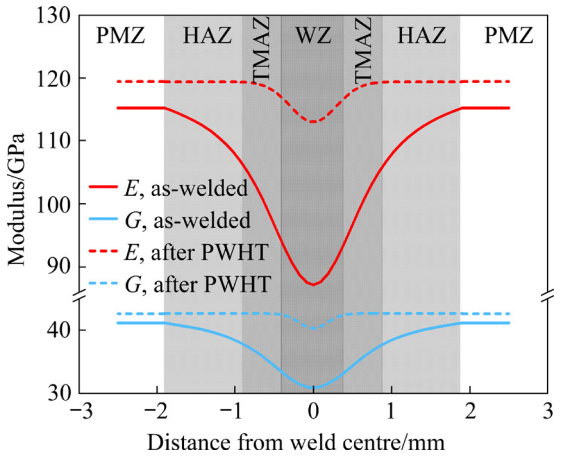

Fig. 7 Modulus variation of TC17 in welding area

The E_{TC17} and G_{TC17} of each zone are different and significantly change after PWHT. Therefore, the non-homogeneity of E_{TC17} and G_{TC17} should be considered when calculating the internal residual stresses in LFW weldments of TC17 titanium alloy using the contour method.

3.5 Residual stress distribution

EDM cutting was performed on welded and PWHTed weldments. The contour of cut surfaces after the data processing is shown in Fig. 8. The gradient of the cut surface deformation around the

weld centre is steep, indicating that significant residual stresses are generated. Then, the contour data and elastic constants in the welding area are substituted into FEA to obtain the internal residual stress distribution of weldments.

In this study, residual stresses are calculated using two methods. In Method 1, the elastic constants in the welding area are considered the same as those of PM. In Method 2, the gradient distribution of phase fraction is considered in the welding area. A path is selected on the cut surface (Fig. 4) to visualize the stress distribution. In order to compare and analyze the two calculations, a local area of 5 mm from the weld centre is selected. The comparison results are shown in Fig. 9.

For the weldments as welded, the residual stress distribution and peak tensile stress location calculated using the two methods are approximately the same. However, the calculated values of residual stresses in the welding area using Method 2 are lower due to the E_{TC17} in the area being smaller than that in PM. Because the E_{TC17} in PMZ does not change during LFW, the calculation results are the same for the two methods.

The average relative error of residual stresses calculated using Method 1 in the welding area is 13.88%. The relative error is the maximum (20.36%) at the weld centre since E_{TC17} in WZ varies the most during LFW.

After PWHT, E_{TC17} in the welding area increases, which is approximately the same as E_{TC17} in PM. Therefore, the relative error of the residual stresses in the welding area calculated using the two methods is only 2.48%. However, in PMZ, the relative error (36.06%) of residual stresses calculated using Method 1 could not be neglected due to the significant variation in E_{TC17} after PWHT.

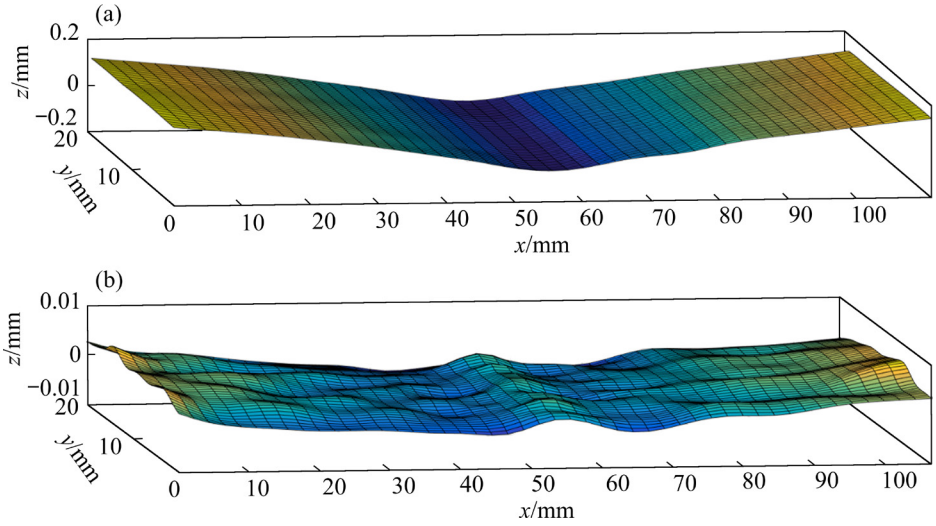

Fig. 8 Contour of cut surfaces: (a) As-welded; (b) After PWHT

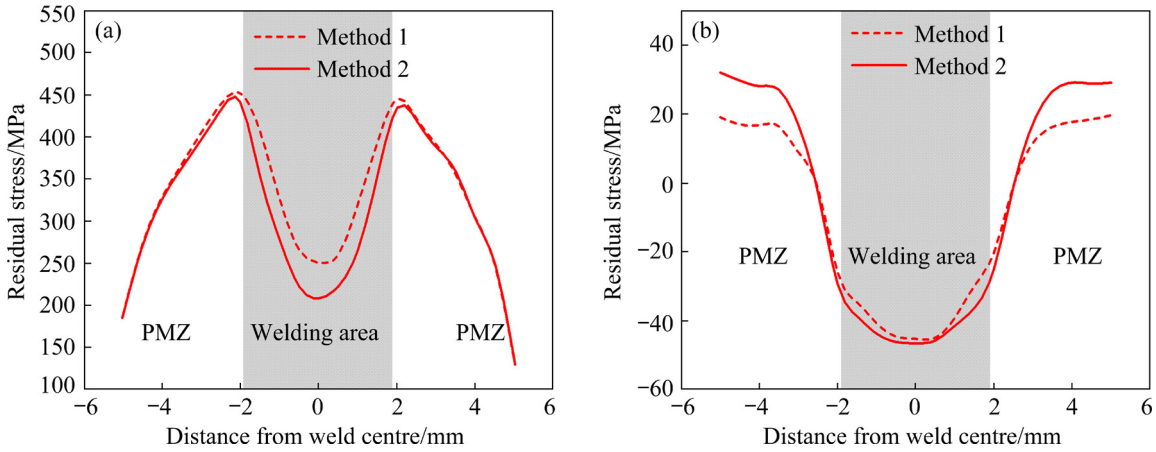

Fig. 9 Residual stresses on path in 5 mm local area: (a) As-welded; (b) After PWHT

Therefore, if the gradient distribution of phase fraction is ignored, there will be an unacceptable error when using the contour method to calculate the internal residual stresses in weldments of TC17 titanium alloy.

The residual stresses on the path (Fig. 4) considering the gradient distribution of phase fraction are shown in Fig. 10. The internal residual stresses are tensile close to the weld centre and compressive on both sides. A local high temperature is generated near the weld centre during LFW, and the cooling speed in the core is significantly lower than that on the surface. This phenomenon indicates that the surrounding material obstructs the core during the volume contraction, resulting in high tensile stresses. The residual stresses rapidly change from tensile to compressive in an area about 6 mm away from the weld centre and gradually turn to zero at the edge of weldment due to the large temperature gradient in the welding area. After PWHT, the residual stresses are eliminated and remain within ~47 MPa.

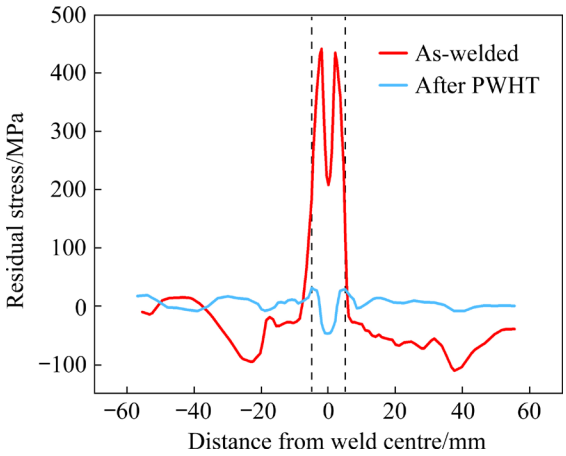

Fig. 10 Overall residual stresses on path

The residual stresses of as-welded specimen in the 5 mm local area are shown in Fig. 9(a). The internal residual stress distribution is symmetric on both sides of the local area and has an "M" shape. The peak tensile stress of ~442 MPa is located in PMZ close to the HAZ side (about 2 mm away from the weld centre). When it is close to the weld centre, the tensile stresses gradually decrease and reach a minimum value of ~208 MPa at the centre. Under the coupling effect of high temperature and frictional deformation in the welding area, the α_p and α_s transform into β. Moreover, dynamic reversion and recrystallization occur, resulting in fine equiaxed grains, which decreases tensile stresses at the weld centre.

As shown in Fig. 9(b), the residual stresses in the welding area transform from tensile to compressive after PWHT. In contrast to residual stresses of as-welded specimen, the peak compressive stress of ~47 MPa is located at the weld centre with a reduction rate of 77.68%. The peak tensile stress in PMZ near the HAZ side reduces to ~30 MPa with a reduction rate of 93.21%. The average compressive residual stress within the 5 mm local area is ~11 MPa, with an overall reduction rate of 87.85%. The internal residual stresses after PWHT are extremely small, and as a result, they could be ignored.

4 Conclusions

(1) The elastic constants (elastic and shear moduli) of TC17 titanium alloy are positively correlated with α phase fraction.

(2) The LFW process results in different microstructure variations in each zone. Fine equiaxed β grains are mainly concentrated in WZ, while severely deformed grains are present in TMAZ. The grain size and morphology in HAZ are similar to those in PMZ, with a typical basket-weave structure.

(3) LFW and PWHT significantly affect the phase fraction of TC17 titanium alloy and induce gradient distribution of phase fraction in the welding area, which is pivotal in calculating the residual stresses. If the gradient distribution of phase fraction is ignored, the maximum relative error after welding is 20.36%, and the maximum relative error after PWHT is 36.06%.

(4) The internal residual stresses in the weldments as-welded have an "M" shape distribution, with tensile stresses in the middle and compressive stresses on both sides. The peak tensile stress of ~442 MPa is located in PMZ close to the HAZ side. After PWHT, residual stresses at the weld centre transform from tensile to compressive.

CRediT authorship contribution statement

Peng HE: Methodology, Visualization, Writing − Original draft preparation; **Yun-xin WU:** Conceptualization; **Tao ZHANG:** Writing − Reviewing and editing; **Song-yi CHEN:** Validation; **Chen ZHANG:** Data curation.

Declaration of competing interest

The authors declare that they have no known competing financial interests or personal relationships that could have appeared to influence the work reported in this paper.

Acknowledgments

This work was supported by the National Natural Science Foundation of China (No. 51975596) and the Fundamental Research Funds for the Central Universities of Central South University, China (No. CX20220285).

References

[1] MCANDREW A R, COLEGROVE P A, BÜHR C, FLIPO B C D, VAIRIS A. A literature review of Ti−6Al−4V linear friction welding [J]. Progress in Materials Science, 2018, 92: 225−257.

[2] BALLAT-DURAND D, BOUVIER S, RISBET M. Deep understanding of the influence of the process parameters during linear friction welding on the joint quality and the microstructural changes of two mono-material titanium alloy joints: The β-metastable Ti−5Al−2Sn−2Zr−4Mo−4Cr (Ti17) and the near-α Ti−6Al−2Sn−4Zr−2Mo (Ti6242) [J]. Metallurgical and Materials Transactions A, 2019, 51: 263−278.

[3] ZHAO Peng-kang, WEI Chen, LI Yan, TAO Jun, ZHANG Chuan-chen, XIAO Xu-dong, ZHANG Min. Effect of heat treatment on the microstructure, microhardness and impact toughness of TC11 and TC17 linear friction welded joint [J]. Materials Science and Engineering A, 2021, 803: 140496.

[4] PANG Hao-yu, LUO Jiao, ZHANG Zhi-gang, HAN Wen-chao, XU Keng-feng, LI Miao-quan. Quantitative analysis of globularization and modeling of TC17 alloy with basketweave microstructure [J]. Transactions of Nonferrous Metals Society of China, 2022, 32(3): 850−867.

[5] SARESH N, PILLAI M G, MATHEW J. Investigations into the effects of electron beam welding on thick Ti−6Al−4V titanium alloy [J]. Journal of Materials Processing Technology, 2007, 192: 83−88.

[6] GENG Pei-hao, QIN Guo-liang, ZHOU Jun, LI Chang-an. Parametric optimization and microstructural characterization of friction welded aeronautic aluminum alloy 2024 [J]. Transactions of Nonferrous Metals Society of China, 2019, 29(12): 2483−2495.

[7] DALGAARD E C. Evolution of microstructure, microtexture, and mechanical properties in linear friction welded titanium alloys [D]. McGill University Montreal, Canada, 2011.

[8] BOYAT X, BALLAT-DURAND D, MARTEAU J, BOUVIER S, FAVERGEON J, OREKHOV A, SCHRYVERS D. Interfacial characteristics and cohesion mechanisms of linear friction welded dissimilar titanium alloys: Ti−5Al−2Sn−2Zr−4Mo−4Cr (Ti17) and Ti−6Al−2Sn−4Zr−2Mo (Ti6242) [J]. Materials Characterization, 2019, 158: 109942.

[9] ZHANG Chuan-chen, ZHANG Tian-cang, JI Ya-juan, HUANG Ji-hua. Effects of heat treatment on microstructure and microhardness of linear friction welded dissimilar Ti alloys [J]. Transactions of Nonferrous Metals Society of China, 2013, 23(12): 3540−3544.

[10] TURNER R, WARD R M, MARCH R, REED R C. The magnitude and origin of residual stress in Ti−6Al−4V linear friction welds: An investigation by validated [J]. Metallurgical and Materials Transactions B, 2012, 43: 186−197.

[11] DAYMOND M R, BONNER N W. Measurement of strain in a titanium linear friction weld by neutron diffraction [J]. Physica B: Condensed Matter, 2003, 325: 130−137.

[12] WITHERS P J, TURSKI M, EDWARDS L, BOUCHARD P J, BUTTLE D J. Recent advances in residual stress measurement [J]. International Journal of Pressure Vessels and Piping, 2008, 85(3): 118−127.

[13] LIU Chuan, DONG Chun-lin. Internal residual stress measurement on linear friction welding of titanium alloy plates with contour method [J]. Transactions of Nonferrous Metals Society of China, 2014, 24(5): 1387−1392.

[14] FRANKEL P, PREUSS M, STEUWER A, WITHERS P J, BRAY S. Comparison of residual stresses in Ti−6Al−4V and Ti−6Al−2Sn−4Zr−2Mo linear friction welds [J]. Materials Science and Technology, 2009, 25(5): 640−65.

[15] HOSSEINZADEH F, LEDGARD P, BOUCHARD P J. Controlling the cut in contour residual stress measurements of electron beam welded Ti−6Al−4V alloy plates [J]. Experimental Mechanics, 2013, 53(5): 829−839.

[16] DEWALD A T, LEGZDINA D, CLAUSEN B, DONALD W B, THOMAS A S, MICHAEL R H. A comparison of residual stress measurements on a linear friction weld using the contour method and neutron diffraction [J]. Experimental and Applied Mechanics, 2012, 4: 183−189.

[17] GADALLAH R, TSUTSUMI S, AOKI Y, FUJII H. Investigation of residual stress within linear friction welded steel sheets by alternating pressure via X-ray diffraction and contour method approaches [J]. Journal of Manufacturing Processes, 2021, 64: 1223−1234.

[18] LI Wen-ya, MA Tie-jun, YANG Si-qian. Microstructure evolution and mechanical properties of linear friction welded Ti−5Al−2Sn−2Zr−4Mo−4Cr (Ti17) titanium alloy joints [J]. Advanced Engineering Materials, 2010, 12(1): 35−43.

[19] WANG S Q, LIU J H, LU Z X, CHEN D L. Cyclic deformation of dissimilar welded joints between Ti−6Al−4V and Ti17 alloys: Effect of strain ratio [J]. Materials Science and Engineering A, 2014, 598: 122−134.

[20] LEE Y T, PETERS M, WELSCH G. Elastic moduli and tensile and physical properties of heat-treated and quenched powder metallurgical Ti−6Al−4V alloy [J]. Metallurgical Transactions A, 1991, 22(3): 709−714.

[21] FRÉOUR S, GLOAGUEN D, FRANÇOIS M, GUILLEN R, GIRARD E, BOUILLO J. Determination of the macroscopic elastic constants of a phase embedded in a multiphase polycrystal−Application to the β-phase of a Ti-17 titanium based alloy [J]. Materials Science Forum, 2002, 404/405/406/407: 723−728.

[22] LEE Y T, WELSCH G. Young's modulus and damping of Ti−6Al−4V alloy as a function of heat treatment and oxygen

concentration [J]. Materials Science and Engineering A, 1990, 128: 77−89.
[23] OGI H, KAI S, LEDBETTER H, TARUMI R, HIRAO M, TAKASHIMA K. Titanium's high-temperature elastic constants through the hcp–bcc phase transformation [J]. Acta Materialia, 2004, 52: 2075−2080.
[24] CHEN Wei, CHEN Chao, ZI Xuhui, CHENG Xiao-fan, ZHANG Xiao-yong, LIN Yong-cheng. Controlling the microstructure and mechanical properties of a metastable β titanium alloy by selective laser melting [J]. Materials Science and Engineering A, 2018, 726: 240−250.
[25] AHMED W, ELHISSI A, JACKSON M J, AHMED E. Precision machining of medical devices [M]//The Design and Manufacture of Medical Devices. Woodhead Publishing, 2012: 59−113.
[26] LEYENS C, PETERS M. Titanium and titanium alloys [M]. Darmstadt: Betz-druck GmbH, 2003: 37−57.
[27] TANE M, OKUDA Y, TODAKA Y, OGI H, NAGAKUBO A. Elastic properties of single-crystalline ω phase in titanium [J]. Acta Materialia, 2013, 61: 7543−7554.
[28] BALLAT-DURAND D, BOUVIER S, RISBET M. Contributions of an innovative post-weld heat treatment to the micro-tensile behavior of two mono-material linear friction welded joints using: The β-metastable Ti−5Al−2Sn−2Zr−4Mo−4Cr (Ti17) and the near-α Ti−6Al−2Sn−4Zr−2Mo (Ti6242) Ti-alloys [J]. Materials Science and Engineering A, 2019, 766: 138334.
[29] MORI T, TANAKA K. Average stress in matrix and average elastic energy of materials with misfitting inclusions [J]. Acta Metallurgica, 1973, 21(5): 571−574.
[30] WENG G J. Some elastic properties of reinforced solids, with special reference to isotropic ones containing spherical inclusions [J]. International Journal of Engineering Science, 1984, 22(7): 845−856.
[31] BENVENISTE Y. A new approach to the application of Mori−Tanaka's theory in composite materials [J]. Mechanics of Materials, 1987, 6(2): 147−157.
[32] PRIME M B, KASTENGREN A L. The contour method cutting assumption: Error minimization and correction [J]. Experimental and Applied Mechanics, 2011, 6: 233−250.
[33] TOPARLI M B, FITZPATRICK M E, GUNGOR S. Improvement of the contour method for measurement of near-surface residual stresses from laser peening [J]. Experimental Mechanics, 2013, 53(9): 1705−1718.
[34] LI Xiao-hong, HE Jian-chao, JI Ya-juan, ZHANG Tian-cang, ZHANG Yan-hua. Study of the microstructure and fracture toughness of TC17 titanium alloy linear friction welding joint [J]. Metals, 2019, 9(4): 430.

考虑相含量的 TC17 钛合金线性摩擦焊中的残余应力

何 鹏[1,2]，吴运新[1,2]，张 涛[1,2]，陈送义[1,2]，张 晨[1,2]

1. 中南大学 轻合金研究院，长沙 410083；
2. 中南大学 极端服役性能精准制造国家重点实验室，长沙 410083

摘 要：为了获得准确的 TC17 钛合金线性摩擦焊中的残余应力，建立 TC17 钛合金弹性常数与相分数之间的数值关系。结合焊接区域的相分数，获得呈梯度分布的弹性常数，并将其引入轮廓法进行计算。结果表明， TC17 钛合金的弹性常数与 α 相分数呈正相关，在宽度约 4 mm 的焊接区域呈现明显的梯度分布特征；若忽略相分数的梯度分布，计算残余应力时相对误差可达 36.06%；修正后的残余应力呈双峰分布，在热影响区边缘处达到峰值，约为 442 MPa。这说明考虑相分数的梯度分布是必要的。

关键词：线性摩擦焊；TC17 钛合金；残余应力；相分数；梯度分布

(Edited by Bing YANG)